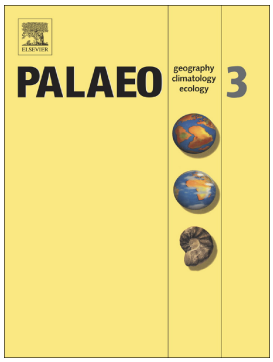


# Subtropical mangrove and evergreen forest reveal Paleogene terrestrial climate and physiography at the North Pole

Jean-Pierre Suc, Séverine Fauquette, Speranta-Maria Popescu, Cécile Robin

PII: S0031-0182(20)30200-5

DOI: https://doi.org/10.1016/j.palaeo.2020.109755

Reference: PALAEO 109755

To appear in: *Palaeogeography, Palaeoclimatology, Palaeoecology*

Received date: 20 December 2019

Revised date: 10 April 2020

Accepted date: 11 April 2020

Please cite this article as: J.-P. Suc, S. Fauquette, S.-M. Popescu, et al., Subtropical mangrove and evergreen forest reveal Paleogene terrestrial climate and physiography at the North Pole, *Palaeogeography, Palaeoclimatology, Palaeoecology* (2020), https://doi.org/10.1016/j.palaeo.2020.109755

# Subtropical mangrove and evergreen forest reveal Paleogene terrestrial climate and physiography at the North Pole

**Jean-Pierre Suc[a*], Séverine Fauquette[b], Speranta-Maria Popescu[c], Cécile Robin[d]**

[a] *Sorbonne Université, CNRS-INSU, Institut des Sciences de la Terre Paris, ISTeP UMR 7193, 75005 Paris, France*

[b] *ISEM, Univ. Montpellier, CNRS, IRD, EPHE, Montpellier, France*

[c] *Geobiostratdata.Consulting, 385 route du Mas Rillier, 69140 Rillieux-la-Pape, France*

[d] *Univ. Rennes, CNRS, Géosciences Rennes-UMR 6118, 35000 Rennes, France*

* Corresponding author

E-mail address: jeanpierre.suc@gmail.com (J.-P. Suc)

**Abstract**

Sedimentological, micropaleontological and geochemical studies of IODP Leg 302 boreholes, M0004A and M0002A, drilled on the Lomonosov Ridge near the North pole, are reported to construct chronostratigraphy and helped unravel Paleogene palaeoclimatic. These studies concluded to a mean annual temperature of sea surface waters ranging between 21 and 25 °C during the Paleocene–Eocene Thermal Maximum and to the occurrence of episodic ice on the Arctic shelf in the earliest Mid-Eocene. Pollen records are characterised by excellent preservation and identification of 112 taxa reveals a subtropical coastal vegetation comprising *Taxodium-Glyptostrobus* swamps alternating with *Avicennia* mangrove. The hinterland was occupied by a subtropical evergreen forest including *Engelhardia* and *Distylium*, occasionally replaced by *Rhodoleia* and *Castanopsis-Lithocarpus*. Climate was reconstructed using the Climatic Amplitude Method, resulting in the following temperature ranges for low elevations: mean annual temperature 18–22 °C, mean temperature of the coldest month 10–14.5 °C, mean temperature of the warmest month 26–27.5 °C, and annual precipitation 1150–1400 mm. Palaeovegetation data allow us to establish climatostratigraphic relationships with the generalized oxygen isotope curve, providing evidence for warm periods (e.g.: Paleocene–Eocene Thermal Maximum, PETM; Early Eocene Climatic Optimum, EECO; Mid Eocene Climatic Optimum, MECO) alternating with cooler periods. We date the latest record of *Avicennia* mangrove in the Arctic Basin to the MECO. The *Azolla* phase did not occur after the EECO but at ~50 Ma during a climatically unstable episode during the thermal optimum. Recurrence of rarely produced and weakly transported *Avicennia* pollen, the exceptional level of preservation of pollen grains, and the high plant diversity indicate that lands of the Lomonosov Ridge were connected to North America in the Ellesmere Island region which, in addition, provided pollen grains of Gymnosperms from high elevations. These physiographic features, suggesting the inflow of altitudinal cold waters into the sea, may solve the apparent

contradiction between possible sea-ice and our reconstructed air temperatures during the Middle Eocene.

**Keywords**

Pollen flora – Climate quantification – Eocene – Climatostratigraphy – IODP 302 – Palaeogeography.

## 1. Introduction

Boreholes M0004A (87°51.996'N, 136°10.644'E) and M0002A (87°55.272'N, 139°21.9'E) of the IODP Leg 302 (Arctic Coring EXpedition: ACEX), located on the Lomonosov Ridge (Jokat, 2005), represent an exceptional sedimentary archive for the reconstruction of Paleocene and Eocene environments and climate at the North Pole (Fig. 1). Many sedimentological, micropalaeontological and geochemical studies of the two boreholes (Backman et al., 2006; Brinkhuis et al., 2006; Sluijs et al., 2006, 2009) set out to identify the chronology and marine environments, despite the fact that the sediments lack calcareous and siliceous microfossils making it impossible to reconstruct the oxygen isotope trend ($\delta^{18}O$) at this location (Sluijs et al., 2006). However, several studies using organic biomarkers provided climatic information on the Paleocene and Eocene from borehole M0004A (Sluijs et al., 2006, 2008; Weijers et al., 2007) and from other sites in the Norwegian–Greenland Sea (Schouten et al., 2008). The presence of pollen grains in these sediments revealed by some authors was looked as promising for the interpretation of terrestrial palaeoenvironments (vegetation, climate) but no detailed analysis followed (Sluijs et al., 2006, 2009). A pollen study of a small interval in the lower part of the series (367.50–390.71 mcd bsf, composite depth below sea floor) only identified 37 taxa referenced to botanical taxonomy in 76 samples (Willard et al., 2019). These disappointing results were probably due to short use of pollen morphology,

which identified only very common taxa in the flora and, as a consequence, the palaeoclimatic values from these data were unreliable. For example, many pollen grains are unidentified in this work and grouped in basic morphological categories such as 'tricolpate', tricolporate reticulate', 'monocolpate', 'tetracolpate', and 'tetracolporate' pollen grains (Willard et al., 2019), including probably several other morphological features belonging to different genera. This approach lessens the palaeoecological and palaeoclimatic significance of a pollen flora as do some general ascriptions to pseudo-genera (e.g., '*Tricolpopollenites*', '*Triatripollenites*', '*Tricolporopollenites*'). For the sake of comparison, we identified 107 botanical taxa in only 17 samples in the Faddeevsky pollen flora (Anjou Islands, part of the New Siberian Islands) which covers almost the same time interval (Fig. 1; Suan et al., 2017). The robustness of reconstructed vegetation and climate in the Arctic region during the Paleocene and Eocene requires a maximum level of knowledge of the composition of the flora, which implies a significant investment in the botanical identification of the pollen grains.

## 2. Material and methods

### *2.1. Material*

Here, our pollen analysis concerns 51 samples: 38 from borehole M0004A and 13 from borehole M0002A, distributed from 401.31 to 270.12 mcd and from 263.81 to 221.02 mcd, respectively. Complete palynological content characterised by an excellent preservation is provided in Appendix A (Supplementary material). The sediments were deposited in a marine environment as supported by the continuous occurrence of dinoflagellate and acritarch cysts. Based on (1) optimal examination of pollen morphology and (2) comparison with specimens from two modern pollen collections (more information in Appendix C of the Supplementary

material) and with photograph databases and specialised papers (both at light microscope and scanning electronic microscope), the flora shows 112 taxa. Eighty-two of the botanical identifications are at the genus level and mostly concern trees, 28 others are at the family level and concern some trees and mainly herbaceous plants. The raw pollen data are shown in a detailed diagram where percentages were calculated with respect to the number of identified pollen grains (comprised between 106 and 231 per sample) (Fig. 2). The complete palynological countings are given in Appendix B (Supplementary material).

*2.2. Methods*

Each sample was processed using a standard soft method: acid digestion (HCl, HF), concentration using $ZnCl_2$ (at density 2.0), and sieving through a 10-µm nylon mesh. A 40-µl volume of residue was mounted between the coverslip and microscope slide using glycerol in order to allow rotation of pollen grains for their identification using an AX10 Zeiss light microscope at x250 and x1,000 magnifications, respectively. The rarely used technique of mounting the residue in glycerol allows some mobility of pollen grains so their different sides can be examined, thus facilitating their morphological examination and their botanical identification.

To forward interpretation of the pollen record, a synthetic diagram was used to group taxa according to the thermal requirements of the genera and families and with respect to their ecological significance (Fig. 3). Percentages of groups of plants are calculated with respect to the number of identified pollen grains minus those of *Pinus* and indeterminable Pinaceae. Plants were grouped according to their required mean annual temperature (MAT) into megatherms (MAT>24 °C), mega-mesotherms (20 °C<MAT<24 °C), mesotherms (14 °C<MAT<20 °C), meso-microtherms (12 °C<MAT<14 °C), and microtherms (MAT<12 °C), as suggested by Nix (1982). Because of the Laurasian trait of the Paleogene flora of the Arctic

region (McIntyre, 1991; McIver and Basinger, 1999; Eberle and Greenwood, 2012; Suan et al., 2017; Salpin et al., 2019), we listed the content in genera and/or families of each thermal group according to the information provided by several syntheses on modern plants from North America, Europe and Asia (e.g.: Thompson et al., 2000; Fang et al., 2011). In addition, the behaviour of many elements of this Laurasian palaeoflora is well-known along the Late Cenozoic in Europe and around the Mediterranean Basin (Suc et al., 2018), which was also used to support their thermal grouping.

The investment in pollen identification and counting meant we were able to use the Climatic Amplitude Method to reconstruct climate conditions during the deposition of the sediments at IODP sites M0004A and M0002A. This method, after comparison with more than 6,000 present-day pollen records distributed worldwide, relies on the relationship between the relative abundance of each individual taxon and the climate because the method accounts not only for the presence/absence criterion but also percentages (Fauquette et al., 1998). The estimated mean annual temperatures (MAT), mean temperatures of the coldest (MTC) and warmest (MTW) months and mean annual precipitation (MAP) concern low-elevation vegetation because meso-microthermal and microthermal taxa (*Cedrus*, *Fagus*, *Tsuga*, *Abies*, *Picea*, plus *Cathaya* and *Podocarpus* which live today at higher elevations in tropical-subtropical regions) were excluded from the process to avoid a cold bias linked to transport from higher elevations. *Pinus*, which may inhabit different vegetation belts, is also excluded from the calculation. The excluded taxa were defined based on the distribution of vegetation today. Indeed, the types of vegetation described in the Early to Middle Eocene in the Arctic region (Suan et al., 2017; Salpin et al., 2019) are found in South-eastern China today at around 25°N and 110 to 120°E (Hou, 1983). In this region, the vertical distribution of the vegetation is characterised, from the base to the top of the massifs by evergreen broad-leaved forest, mixed evergreen and deciduous (*Betula*, *Acer*) broad-leaved forest,

*Cathaya*/*Tsuga* forest, *Picea*/*Abies* forest and high mountain meadows (Hou, 1983). In the Climatic Amplitude Method, the estimates for each climatic parameter are given as an interval (minimum and maximum values of the parameter) and a most likely value (MLV) corresponding to a weighted mean, a statistical calculation tested on modern pollen data which has provided reliable results and which is given in the text (Fauquette et al., 1998).

## 3. Results and discussion

### *3.1. Vegetation and climate*

Remarkable components of the coastal vegetation are *Avicennia* and *Casuarina* which grew in mangrove areas, as they do in Florida today where they contribute to a mosaic vegetation with the bald cypress (*Taxodium distichum*) swamps (Tomlinson, 1986; Willard et al., 2001). Herbaceous and aquatic plants signal the existence of marshes, perhaps also inhabited by Cyrillaceae-Clethraceae, *Myrica* and *Nyssa* (Figs. 2, 3; Tomlinson, 1986; Willard et al., 2001). The monotypic *Avicennia* mangrove apparently competed the cypress swamps mainly illustrated by papillate pollen grains of Cupressaceae (i.e., the former 'Taxodiaceae') (Figs. 2, 3) that, on the basis of morphological pollen examination and information from Eocene macrofloras of the Arctic region (see also Appendix C in the Supplementary material), we consider to represent a *Taxodium-Glyptostrobus* cluster. However, *Avicennia* mangrove is underrepresented in the pollen data: any increase in *Avicennia* pollen that offset a decrease in *Taxodium-Glyptostrobus* was continually minimized by the limited quantity of pollen produced by *Avicennia* and its low dispersal ability (Somboom, 1990; Phuphumirat et al., 2016). As a consequence, *Avicennia* mangrove is underrepresented in the pollen data. Behind the coastal vegetation, a rich evergreen forest developed dominated by Juglandaceae (*Engelhardia*, *Platycarya*, *Rhoiptelea*, cf. *Alfaroa*),

Fagaceae (*Castanopsis-Lithocarpus*), Hamamelidaceae (*Distylium Rhodoleia*, *Matudaea*, *Embolanthera*, *Fothergilla*, *Loropetalum*), Celastraceae, Menispermaceae, Sapotaceae, Malvaceae (*Craigia*, *Bombax*-type), Leguminosae (*Acacia*-type), Rubiaceae (*Canthium*-type, *Mussaenda*-type, *Uncaria*-type), Icacinaceae (*Mappianthus*), Ulmaceae (cf. *Phyllostylon*), Podocarpaceae (*Dacrydium*), Vitaceae (*Cissus*), Euphorbiaceae, Arecaceae, etc. and Sciadopityaceae (*Sciadopitys*) (Fig. 2). Cooler biotopes were inhabited by deciduous elements (*Alnus*, *Carpinus*, *Carya*, *Pterocarya*, *Liquidambar*, *Quercus*, *Ulmus*, *Zelkova*, etc.) and by some gymnosperms such as *Cathaya* and *Podocarpus*, probably located at mid-elevation (Fig. 2). The relatively smaller proportions of pollen grains of meso-microtherms (*Fagus*, *Cedrus*, *Tsuga*) and microtherms (*Abies*, *Picea*)=probably originated from higher elevations (Fig. 2). Although *Cupressus-Juniperus*-type (Cupressaceae) is a major constituent of the pollen flora (Fig. 2), its status in the vegetation is difficult to qualify because the pollen cannot be identified to the genus level. This taxon, abundant in some warmer phases (Fig. 3), may partially refer to some mega-mesotherms such as *Chamaecyparis*, *Taiwania*, *Sabina*, etc. Pollen grains of pine, which are usually over-represented in marine sediments, are not abundant in the record, thereby excluding an important role for this genus in the vegetation and/or revealing the proximity of the coast.

The occurrence interval of *Avicennia* (382.44–235.88 mcd; Fig. 2) delimits a warm period characterised by peaks of both megathermal and mega-mesothermal plants. We have identified eight samples or clusters of samples where *Avicennia* pollen is present in significant percentage (more often from more than 1% to more than 3%: see Appendix A in the Supplementary material) associated with eight maxima of the reconstructed mean annual temperature (MAT) comprised between 20 °C and 22 °C with overall, relatively reduced confidence intervals. Simultaneously, the reconstructed mean temperatures of the coldest and warmest months (MTC and MTW, respectively) are generally high (14–15 °C and 27–28 °C,

respectively; Fig. 3). Light grey bands are drawn to highlight these warm periods (Fig. 3). They coincide with the significant presence of megathermal and mega-mesothermal plants, maxima of MAT and maxima of MTC also characterised by relatively reduced confidence intervals. The estimated mean annual precipitation (MAP) is high, comprised between 1150 and 1400 mm. Such warm and wet climatic conditions exist today in South-eastern China at ~22 to 27°N (Hou, 1983) and in Florida up to latitude ~28°N (Climate-Data website). In addition to its weighty significance as representative of mangrove vegetation (see above), *Avicennia* probably influenced upwards the calculated temperatures and contributed to increase amplitude between successive maxima and minima. Identification of megathermal taxa as *Avicennia* constitutes a striking example of advances expected from pollen floras when they are analysed off the beaten track. Four major cooler episodes were identified based on the absence of megathermal plants, the decreasing abundance of mega-mesotherms and the increase in *Cathaya* and *Podocarpus*, indicated by dark grey bands in (Fig. 3). The corresponding reconstructed MAT falls to around 20 °C while the mean temperatures of the coldest and warmest months drop to 11–12 °C and ~26 °C, respectively (Fig. 3). MAP does not reveal significant variations, as supported by its narrow confidence intervals: its maxima and minima are often independent of temperature changes (Fig. 3). A relatively unstable episode with significant temperature fluctuations and a slight decrease in precipitation lasts from 302.435 to 295.46 mcd (Fig. 3). This relatively unstable warm episode is sandwiched between two warmer phases, also characterised by the biggest increase in *Castanopsis-Lithocarpus* pollen, probably expressing the peak development of the Eocene Arctic subtropical evergreen forest.

*3.2. Climatostratigraphy*

The interval of occurrence of the subtropical dinoflagellate cyst *Apectodinium augustum* (387–378.5 mcd in borehole M0004A) is generally considered to encompass the Paleocene–Eocene Thermal Maximum (PETM), characterised by a $\delta^{13}C$ negative excursion (Sluijs et al., 2006). In fact, the pollen record and quantified climate show a thermal optimum (MLVs of: MAT = 21.2 °C; MTC = 13.7 °C; MTW = 27.4 °C) within this interval at 382.44 mcd which can be correlated with the brief PETM as illustrated by the generalized oxygen isotope curve (Fig. 3; Vandenberghe et al., 2012). The resulting climatostratigraphy (correlations are indicated by the blue patches for the major warmer phases and dotted lines for the secondary warmer phases) shows which thermal peaks of the oxygen isotope curve and pollen data can be associated within the pre-established chronostratigraphy (Fig. 3). Here, the PETM is marked by the first occurrence of *Avicennia*, the prevalence of *Taxodium-Glyptostrobus*, the momentary absence of *Cathaya*, *Podocarpus*, meso-microthermal and microthermal trees and a brief peak in *Cupressus-Juniperus*-type pollen, during an overall drop in precipitation (Fig. 3). Such estimated annual precipitation shows similar ranges to those reported by Eldrett et al. (2014) on the basis of pollen record at lower latitude (Central North Sea). Our calculated temperatures for the PETM from borehole M0004A pollen data are in agreement with the values we obtained for the same period in Arctic Siberia and Canada (Suan et al., 2017; Salpin et al., 2019) but are significantly higher than those deduced from a preceding pollen record (Willard et al., 2019). In their study, Willard et al. (2019) estimate mean annual temperatures between 16 and 18 °C at the beginning of the PETM. The discrepancy can be easily explained by the above-mentioned weakness in pollen identification. On the opposite, our high temperatures are in line with the high MAT (Weijers et al., 2007) and sea surface temperatures (SST) based on the relative distribution of branched glycerol dialkyl glycerol tetraether (GDGT) membrane lipids derived from bacteria thriving in soils recovered from the same Eocene strata in borehole M0004A (Sluijs et al., 2006, 2008). Indeed, for the PETM,

Weijers et al. (2007) indicate mean annual temperatures between 21 and 25 °C (only the end of the PETM shows lower MAT between 18 and 21 °C) that correlates well with the estimates of SST of Sluijs et al. (2006) based on $TEX_{86}$ (between 21 and 23 °C and around 17/18 °C at the end of the PETM). MAT estimated by Weijers et al. (2007) are thus higher than ours and all the more higher than estimates of Willard et al. (2019).

The section shows two nearby negative excursions of $\delta^{13}C$ at 368.94–368.79 and ~368.00 mcd, respectively. The lower excursion is considered to correspond to the Eocene Thermal Maximum 2 (ETM2) (Sluijs et al., 2009). Our pollen record points to warmer conditions in two samples at 368.395 and 367.535 mcd, marked by *Avicennia* pollen, frequent Arecaceae (palms) and abundant Cupressaceae (including *Taxodium-Glyptostrobus* and *Cupressus-Juniperus*-type) pollen grains, resulting in a peak in the temperature curves (MLVs of: MAT = 21.6–22 °C; MTC = 14 °C; MTW = 27.4 °C; Fig. 3).

According to the sedimentation rate estimated for the lower part of borehole M0004A above the PETM (12.7 m/Myr) (Backman et al., 2008), the Eocene Thermal Maximum 3 (ETM3) would be expected to occur at depth 355 mcd, i.e. within the interval 367.40–345.60 mcd not recovered by coring and consequently devoid of samples.

Surprisingly, the Early Eocene Climatic Optimum (EECO), clearly visible in the generalized oxygen isotope curve through two temperature maxima interrupted by an abrupt cooling episode (Vandenberghe et al., 2012), was not previously clearly identified in borehole M0004A. This is all the more surprising as the *Azolla* phase, assumed to follow the EECO, is located from 304 to 298.9 mcd in the borehole (Brinkhuis et al., 2006). Our pollen record shows two major expansions of the subtropical vegetation at 318.86–313.41 and 292.285–282.055 mcd, mainly represented by *Avicennia* mangrove (>2% in the lower interval, >3% in the upper interval), *Taxodium-Glyptostrobus* swamps, and a higher incidence of *Castanopsis-Lithocarpus* in the evergreen forest and the other subtropical Cupressaceae (Fig. 3). The other

subtropical Cupressaceae (including *Cupressus-Juniperus*-type) could also have played an important role in the evergreen forest. The reconstructed temperatures reveal two successive prominent plateaus of about 21.6 and 21.3 °C for MAT, ~14 °C and 14.3–14.4 °C for MTC, 27.4 °C and ~27.3 °C for MTW. These two thermal maxima are separated by a cooler episode (313.41–292.285 mcd) corresponding to a reduction in megatherms and mega-mesotherms combined with a wider representation of meso-microtherms and microtherms plus herbaceous plants. The cooling episode was itself interrupted with brief warmings (Fig. 3). The MAT rose to 18.4 °C, MTC to 10.4 °C and MTW to 26 °C (Fig. 3). The MTW obtained from pollen flora is consistent with the drop in summer SST (from 25 °C to 17 °C) revealed by alkenones between 299.74 and 299.14 mcd (Weller and Stein, 2008), also suggesting marked temperature variability during the unstable episode emphasized by the pollen flora. The bimodal shape of the warmer episode and the secondary temperature elevations in the sandwiched unstable period resemble the oxygen isotope record of the EECO (Vandenberghe et al., 2012). Therefore, we propose to climatostratigraphically correlate the 318.86–282.055 mcd interval of borehole M0004A with the EECO (Fig. 3). This correlation is also supported by the elevated percentages of *Avicennia*, *Castanopsis-Lithocarpus* and *Taxodium-Glyptostrobus* in the uppermost part of borehole M0004A before their abrupt decrease in the last sample (270.12 mcd) (Fig. 3).

The pollen diagram of borehole M0002A reveals the warm episode at the top of the record with the last occurrence of *Avicennia* (<1%) and *Casuarina* associated with dominant *Taxodium-Glyptostrobus* and reduced *Castanopsis-Lithocarpus* (Figs. 2, 3). Reconstructed temperatures are again high: MAT 20.5–21.3 °C, MTC 13.8–14.5 °C and MTW 26.4–27.3 °C (Fig. 3). By correlating the last warm event with the Mid Eocene Climatic Optimum (MECO) at about 40 Ma, this pollen record may help settle the debate concerning the exact age of the Paleogene beds in borehole M0002A (Backman et al., 2008; Poirier and Hillaire-Marcel,

2011) in favour of a short gap in sedimentation as proposed by Poirier and Hillaire-Marcel (2011) (Fig. 4; Table 1). The preceding fluctuating warm episodes (263.815–250.065 mcd) could thus be correlated with the warmer peaks of oscillations centred on ~42 Ma (Vandenberghe et al., 2012).

Studies of terrigenous sands propose that sea ice initiated in the Arctic Basin at about 46 Ma (St John, 2008; Weller et al., 2008), based on the original age model (Backman et al., 2008) (i.e., after 42 Ma according to the revised age model; Poirier and Hillaire-Marcel, 2011). The occurrence of ice-rafted debris and the abundance of sea-ice-dependent fossil diatoms (*Synedropsis* sp.) lowered the onset of episodic ice on the Arctic shelf at 47.5 Ma (St John, 2008). The intervals with abundant ice-rafted debris and sea-ice diatoms (249.5–248.5, 243.5–236, and 232–225.5 mcd; Stickley et al., 2009) correspond to cooler periods which, in our reconstruction, are characterised by relatively low mean temperature of the coldest month (~10.4 °C). However, the development of seasonal sea ice during these cooler intervals is not really consistent with surviving *Taxodium-Glyptostrobus* swamps on the shoreline and with the subtropical evergreen forest (including *Castanopsis-Lithocarpus*, *Engelhardia*, *Distylium*, *Rhodoleia*, *Platycarya*, and *Nyssa*) which continued to prevail (Fig. 2). Nevertheless, two of the nine current *Synedropsis* species are warm-water species which can be distinguished from the sea-ice *Synedropsis* based only on two criteria (Stickley et al., 2009), the solitary or colonial life-forms, respectively, and valve dimensions. The authors of the study themselves point out that it would be risky to conclude on the ecological preference of the fossil *Synedropsis* based on these two criteria as they are not sufficiently robust. In any case, the occurrence of some ice at the North Pole at around 47.5 Ma is also seriously challenged by relatively high SST (15–20 °C) coeval with increased ice-rafting debris and/or abundant sea-ice-dependent diatoms (Weller et al., 2008; Stein et al., 2015). The first appearance of ice in the northernmost regions is a highly controversial matter. It is proposed to have occurred

between about 38 and 30 Ma by Eldrett et al. (2007) under the form of ephemeral continental ice rather than solely sea ice, an interval deferred to about 33– 26 Ma by Tripati and Darby (2018) despite intermittent initiating circum-Arctic ice from 47 to 42 Ma.

### *3.3. The* Azolla *event*

An *Azolla* phase in borehole M0004A including four maxima of massulae is described between 304 and 298.90 mcd (Brinkhuis et al., 2006). It is usually correlated with a similar event, although with some differences, composed of three maxima distributed along a 21 m thick layer in borehole 913B (Norvegian–Greenland Sea) (Brinkhuis et al., 2006), which encompasses the C22n/C21r chron boundary (Eldrett et al., 2004; Barke et al., 2012) dated to 48.96 Ma (Vandenberghe et al., 2012). Such *Azolla* blooms have been recorded in many locations in the Arctic and Nordic seas and are considered coeval despite the lack of independent dating except for boreholes 913B (Eldrett et al., 2004; Barke et al., 2012) and 338 (Eldrett and Harding, 2009). A single event at the scale of the Northern basins has yet been described, and is considered to have lasted about 800,000 years between 49 and 48 Ma, implying significant freshwater inputs from the land into the Arctic Basin, which then spilled over into the adjacent seas, and involved sustained freshening of surface waters (Brinkhuis et al., 2006; Barke et al., 2012). It has been suggested that this *Azolla* phase depended on the rate of exchange between the Arctic Basin and adjacent seas (Brinkhuis et al., 2006). However, *Azolla* massulae are recorded in turbidites at Site 338 that led Eldrett and Harding (2009) to consider that sediment mass transport from the shelf may be the cause of their occurrence, perhaps in addition or at the place of surface water current from the Arctic Ocean.

Our study enabled us to check for this event at the same depth (302.435–297.72 mcd; Fig. 3; Table 1) in borehole M0004A, marked by abundant massulae and microspores. In our climatostratigraphic interpretation of the pollen record and quantified climate, the *Azolla*

phase did not occur after the EECO as previously proposed but during the climatically unstable episode within this climatic optimum with slightly lower MAT. This is consistent with the 3 °C rise in the sea surface temperature indicated after the termination of the *Azolla* phase (Brinkhuis et al., 2006). At Caribou Hills, an exposed section in the Beaufort-Mackenzie Basin (Fig. 1), two maxima of *Azolla* microspores are recorded just after a warm episode (Salpin et al., 2019) which we correlate with the lower part of the EECO. A fairly detailed pollen record is available, although of poor botanical quality, originating from a borehole in the Beaufort-Mackenzie Basin (Taglu G-33) which displays the *Azolla* phase (Brinkhuis et al., 2006). In the present borehole, the *Azolla* phase is sandwiched between two warmer episodes marked by pollen of thermophilous plants (Staplin, 1976). This *Azolla* phase can thus be ascribed to the cooler episode within the EECO. We believe that a single *Azolla* pulse, which was too hastily correlated at the scale of the Northern basins, should be seriously called into question.

We observed (1) a minor input of *Azolla* microspores at 392.91–390.21 mcd a little before the PETM (Fig. 3), and (2) a younger influx of *Azolla*, marked by sporangia, in the exposed Mid-Eocene Belkovsky section (Anjou Islands, part of the New Siberian Islands) (Suan et al., 2017). Our records complete the occurrence of somewhat younger *Azolla* blooms in the Denmark region (Collinson et al., 2010). Far from challenging the assumption that synchroneity may characterise some *Azolla* layers linked with a generalised pulse in the Northern region (Brinkhuis et al., 2006; Moran et al., 2006), the age of the major episode in borehole M0004A should be lowered and its concept reappraised, as suggested at a wider latitudinal scale by Collinson et al. (2010). In borehole M0004A, the *Azolla* phase is also marked by a significant decline in the frequency of the marine dinoflagellate cysts (Brinkhuis et al., 2006). As the event is linked to a marked drop in temperature that affected the sea (Sluijs et al., 2006) and the land (Fig. 3), a lowering of sea level can be assumed, which

would extend the influence of deltas farther offshore. A lowering of sea level was also considered by Eldrett et al. (2009) on the basis of the above mentioned turbidites at Site 338. Indeed, fossil records of *Azolla* (including massulae and microspores) are known from the Roussillon Basin (South of France) (Florschütz and Menéndez Amor, 1960) and belong to the marine-continental transition of an Early Pliocene delta (Clauzon et al., 2015). A Late Holocene example comes from the Nile Delta where *Azolla* remains (megaspores, microspores and massulae) were recorded in marine to continental sediments (Leroy, 1992). The rapid conspicuous unstable episode intercalated in EECO may have caused a large enough drop in sea level in the Arctic Basin to increase progradation of deltas and increased offshore transport of this common free-floating *Azolla* fern. In this way, the invasion of *Azolla* remains in the Arctic Basin could be the earlier localized sign of a forthcoming more generalized invasion at the beginning of Mid-Eocene.

### *3.4. Palaeogeographic inferences*

The remarkable preservation of pollen grains in boreholes M0004A and M0002A and particularly the occurrence of the infrequent and weakly disseminated *Avicennia* pollen (Somboom, 1990; Phuphumirat et al., 2016) imply that land bordered the coring sites. The low frequency of *Pinus* also supports this assumption (Fig. 2). Samples originating from the warmer phases contain pollen concentration ranging from 1,300 to 2,650 pollen grains/gram (i.e., 2,360 to 4,780 pollen grains/cm$^3$) of sediment, consistent with previous estimates of the total content of terrestrial (including spores) palynomorphs (Sluijs et al., 2008; Willard et al., 2019. Such pollen concentrations are observed in modern sediments in various regions located from a few kilometres to 40 km from the shoreline (Heusser, 1988; Beaudouin et al., 2007). These data imply that land existed nearby on the Lomonosov Ridge, confirming prior signs of land in the vicinity (Sluijs et al., 2009; O'Regan et al., 2008), and corresponding to a

string of islands and peninsulas joining the Ellesmere to New Siberian islands, as already proposed by Eberle and Greenwood (2008) (Fig. 5). Overall, the three Lower Eocene pollen floras from the Arctic region we studied (Faddeevsky: Suan et al., 2017; Caribou Hills: Salpin et al., 2019; M0004A) are almost the same. However, some minor differences, such as the significant proportion of *Castanopsis-Lithocarpus* and Hamamelidaceae (*Distylium*, *Rhodoleia*) in the evergreen forest leads us to envisage a closer resemblance between the ACEX and Faddeevsky pollen floras. The ACEX flora also resembles the Ellesmere flora (macroremains and pollen grains: McIntyre, 1991; McIver and Basinger, 1999; Eberle and Greenwood, 2012). Similarly, these floras contain genera (e.g., *Cathaya*, *Tsuga*, *Abies*, *Picea*) which inhabited elevated belts of the Verkhoyansk Chain on the Asian side (Franke and Hinz, 2009), and of the Eurekan Range on the North American side (Harrison et al., 1999; von Gosen et al., 2019), at the top of which snow and/or ice were probable. Pollen grains of altitudinal trees were certainly transported into the Arctic Basin by rivers and this mode of transport is also likely for the macroremains of elevated trees recorded in sandstones (Eberle and Greenwood, 2012). Considering the location of the ACEX boreholes in the southern part of the Lomonosov Ridge, the Ellesmere Range can probably be regarded as the source of pollen of elevated trees, their transport by river to our study sites was probably facilitated by the presence of a peninsula (Fig. 5).

### *3.5. Updated ACEX Eocene chronology*

Pollen flora and climatostratigraphy led us to re-examine and somewhat modify the age model of boreholes M0004A and M0002A based on recognition of five major warm phases and their correlation with the generalized oxygen isotope curve (Fig. 3; Vandenberghe et al., 2012). The sedimentary record of borehole M0004A should run from ~57 Ma to ~48 Ma and the concerned part of borehole M0002A from ~42 to ~40 Ma (Figs. 3 and 4). Secondary

climatostratigraphic correlations with the oxygen isotope curve can be added peak by peak for the warmer ones (Fig. 3). A revised sedimentation rate of the Paleogene sediments from ACEX is proposed (Fig. 4; Table 1). About 6 Myrs are hypothesized to be missing in the sedimentary continuity of these boreholes.

There is no pollen record to provide information on changes in vegetation during the 48–42 Ma time span linked to climate deterioration, i.e. from EECO to MECO. However, the surviving megatherms (including *Avicennia*) in the M0002A pollen flora (Figs. 2, 3) suggest that these taxa persisted as relicts on the shorelines of the Arctic Basin during the period 49–40 Ma. Temperatures reconstructed from pollen data are significantly higher than those obtained from leaf analysis (West et al., 2015). It is not surprising that a highly diverse pollen flora originating from low elevations indicate more elevated temperatures than a macroflora, the disparity being extended by the biases existing between the methods of calculation as illustrated by a comparative appraisal of an Early Pleistocene locality (Girard et al., 2019).

According to the generalized oxygen isotope curve (Vandenberghe et al., 2012), the MECO was a prominent but brief warm fluctuation. A better understanding of the thermal amplitude of the Mid-Eocene climatic fluctuations will probably help solve the apparent contradiction between the ice-rafted debris and sea-ice diatoms (which are perhaps not species linked to sea ice; Stickley et al., 2009) on the one hand and the pollen data on the other hand. As a possible way to resolve this matter the apparent contradiction between the ice-rafted debris and sea-ice diatoms on the one hand and the pollen data on the other hand if the palaeoecological interpretation of the diatom *Synedropsis* is confirmed, the fluvial transport of ice-rafted debris from high relief areas should be considered as well as the inflow of altitudinal cold waters into the sea. These waters could have facilitated the local dissemination of such diatoms which require low temperatures.

## 4. Conclusion

Pollen record allowed vegetation reconstruction from coastal area to high relief (Figs. 2, 3): competing *Avicennia* mangrove and *Taxodium-Glyptostrobus* swamps on the coastline; hinterland inhabited by subtropical evergreen forest (*Engelhardia*, *Distylium*, *Rhodoleia*, *Castanopsis-Lithocarpus*, etc.); deciduous warm-temperate forest (*Quercus*, *Carpinus*, *Carya*, *Ulmus*, *Zelkova*, etc.); conifer belts (*Cathaya*, *Podocarpus*, *Tsuga*, *Abies*, *Picea*).

Maxima in *Avicennia* pollen mark the warmer periods alternating with cooler phases, the climate of which has been quantified for low elevation lands (MAT: 18–22 °C; MTC: 10–14.5 °C; MTW: 26–27.5 °C; MAP: 1150–1400 mm; Fig. 3). On the whole they are consistent with estimated SST.

Curves of ecological groups shown in the synthetic pollen diagram and reconstructed temperatures allow climatostratigraphic correlations with the generalized oxygen isotope curve: PETM, ETM2, the three phases of EECO, and MCO are evidenced as major climatic events (Fig. 3). This climatostratigraphy results in updating the ACEX Eocene chronology (Fig. 4).

In borehole M0004A, the *Azolla* phase occurred during an unstable episode within the EECO (Fig. 3), differentiating this local event from a more regional episode at the Lower–Middle Eocene transition.

Physiography of the region is specified: lands existed near the cored sites along the Lomonosov Ridge with probable connection with the Ellesmere Range (Fig. 5), the elevated relief of which could explain the fluvial transport to the Arctic Basin of altitudinal Gymnosperm pollen and ice-rafted debris. Input of cold waters originating from high relief could have caused the local development of sea-ice diatoms.

Finally, this pollen study helps answer certain questions raised after the first set of studies on the ACEX Eocene succession (Stein et al., 2015), in particular the uncertainties concerning

the age model of boreholes M0004A and M0002A illustrated for instance by the poor recognition of the EECO before this work was completed.

**Acknowledgements**

IODP agreed this study and the Bremen Core Repository provided the samples thanks to the aid of Dr. Walter Hale and his staff. The study benefited from a financial grant from IODP-France. O. Boudouma assisted us at the scanning electronic microscope. The Herbarium of the National Museum of Natural History Paris and the Herbarium of the Lyon University provided stamens of modern plants. The manuscript greatly benefited from the constructive review by anonymous referees and the journal editor Prof. Howard Falcon-Lang.

**References**

Backman, J., Jakobsson, M., Frank, M., Sangiorgi, F., Brinkhuis, H., Stickley, C., O'Regan, M., Løvlie, R., Pälike, H., Spofforth, D., Gattacecca, J., Moran, K., King, J., Heil, C., 2008. Age model and core-seismic integration for the Cenozoic Arctic Coring Expedition sediments from the Lomonosov Ridge. Paleoceanography 23, PA1S03, doi:10.1029/2007PA001476.

Backman, J., Moran, K., McInroy, D.B., Mayer, L.A., and the Expedition 302 Scientists, 2006. Sites M0001–M0004. Proc. Integr. Ocean Drill. Program, vol. 302, 1–169.

Barke, J., van der Burgh, J., van Konijnenburg-van Cittert, J.H.A., Collinson, M.E., Pearce, M.A., Bujak, J., Heilmann-Clausen, C., Speelman, E.N., van Kempen, M.M.L., Reichart, G.-J., Lotter, A.F., Brinkhuis, H., 2012. Coeval Eocene blooms of the freshwater fern *Azolla* in and around Arctic and Nordic seas. Palaeogeogr. Palaeoclimatol. Palaeoecol. 337–338, 108–119.

Beaudouin, C., Suc, J.-P., Escarguel, G., Arnaud, M., Charmasson, S., 2007. The significance of pollen signal in present-day marine terrigenous sediments: The example of the Gulf of Lions (western Mediterranean Sea). Geobios 40, 159–172.

Brinkhuis, H., Schouten, S., Collinson, M.E., Sluijs, A., Sinninghe Damsté, J.S., Dickens, G.R., Huber, M., Cronin, T.M., Onodera, J., Takahashi, K., Bujak, J.P., Stein, R., van der Burgh, J., Eldrett, J.S., Harding, I.C., Lotter, A.F., Sangiorgi, F., van Konijnenburg-van Cittertn H., de Leeuw, J.W., Matthiessen, J., Backman, J., Moran, K., and the Expedition 302 Scientists, 2006. Episodic fresh surface waters in the Eocene Arctic Ocean. Nature 441, 606–609.

Clauzon, G., Le Strat, P., Duvail, C., Do Couto, D., Suc, J.-P., Molliex, S., Bache, F., Besson, D., Lindsay, E.H., Opdyke, N.D., Rubino, J.-L., Popescu, S.-M., Haq, B.U., Gorini, C., 2015. The Roussillon Basin (S. France): A case-study to distinguish local and regional events between 6 and 3 Ma. Mar. Pet. Geol. 66, 18–40.

Climate-Data. Climate data for cities worldwide. https://www.climate-data.org.

Collinson, M.E., Barke, J., van der Burgh, J., van Konijnenburg-van Cittert, J.H.A., Heilmann-Clausen, C., Howard, L.E., Brinkhuis, H., 2010. Did a single species of Eocene *Azolla* spread from the Arctic Basin to the southern North Sea? Rev. Palaeobot. Palynol. 159, 152–165.

Eberle, J.J., Greenwood, D.R., 2012. Life at the top of the greenhouse Eocene world– A review of the Eocene flora and vertebrate fauna from Canada's High Arctic. Geol. Soc. Amer. Bull. 124, 3–23.

Eldrett, J.S., Greenwood, D.R., Polling, M., Brinkhuis, H., Sluijs, A., 2014. A seasonality trigger for carbon injection at the Paleocene–Eocene Thermal Maximum. Climate of the Past, 10, 759–769.

Eldrett, J.S., Harding, I.C., 2009. Palynological analyses of Eocene to Oligocene sediments from DSDP Site 338, Outer Vøring Plateau. Mar. Micropaleontol. 73, 226–240.

Eldrett, J.S., Harding, I.C., Firth, J.V., Roberts, A.P., 2004. Magnetostratigraphic calibration of Eocene–Oligocene dinoflagellate cyst biostratigraphy from the Norwegian–Greenland Sea. Mar. Geol. 204, 91–127.

Eldrett, J.S., Harding, I.C., Wilson, P.A., Butler, E., Roberts, A.P., 2007. Continental ice in Greenland during the Eocene and Oligocene. Nature 446, 176–179.

Fang, J., Wang, Z., Tang, Z., 2011. Atlas of woody plants in China. Distribution and climate. Higher Education Press, Beijing, Springer, Heidelberg; vol. 1, 1072 pp.; vol. 2, 1902 pp.

Fauquette, S., Guiot, J., Suc, J.-P., 1998. A method for climatic reconstruction of the Mediterranean Pliocene using pollen data. Palaeogeogr. Palaeoclimatol. Palaeoecol. 144, 183–201.

Florschütz, F., Menéndez Amor, J., 1960. Une *Azolla* fossile dansq les Pyrénées Orientales. Pollen et Spores 2, 2, 285–292.

Franke, D., Hinz, K., 2009. Geology of the Shelves surrounding the New Siberian Islands, Russian Arctic. Stephan Mueller Spec. Publ. Ser. 4, 35–44.

Girard, V., Fauquette, S. Adroit, B., Suc, J.-P., Leroy, S.A.G., Ahmed, A., Paya, A., Ali, A., Paradis, L., Roiron, P., 2019. Fossil mega- and micro-flora from Bernasso (Early Pleistocene, southern France): A multimethod comparative approach for paleoclimatic reconstruction. Rev. Palaeobot. Palynol. 267, 54–61.

Harrison, J.C., Mayr, U., McNeil, D.H., Sweet, A.R., McIntyre, D.J., Eberle, J.J., Harington, C.R., Chalmers, J.A., Dam, G., Nøhr-Hansen, H., 1999. Correlation of Cenozoic sequences of the Canadian Arctic region and Greenland; implications for the tectonic history of northern North America. Bull. Canadian Petrol. Geol. 47, 223–254.

Heusser, L.E., 1988. Pollen distribution in marine sediments on the continental margin off Northern California. Mar. Geol. 80, 131–147.

Hou, H.-Y., 1983. Vegetation of China with reference to its geographical distribution. Ann. Missouri Bot. Gard. 70, 509–549.

Jokat, W., 2005. The sedimentary structure of the Lomonosov Ridge between 88°N and 80°N. Geophys. J. Int. 163, 698–726.

Leroy, S.A.G., 1992. Palynological evidence of *Azolla nilotica* Dec. in recent Holocene of the eastern Nile Delta and palaeoenvironment. Veg. Hist. Archaeobot., 1, 43–52.

McIntyre, D.J., 1991. Pollen and spore flora of an Eocene forest, Eastern Axel Heiberg Island, N.W.T. Geol. Surv. Canada Bull. 403, 83–98.

McIver, E.E., Basinger, J.F., 1999. Early Tertiary floral evolution in the Canadian High Arctic. Ann. Missouri Bot. Gard. 86, 523–545.

Moran, K., Backman, J., Brinkhuis, H., Clemens, S.C., Cronin, T., Dickens, G.R., Eynaud, F., Gattacceca, J., Jakobsson, M., Jordan, R.W., Kaminski, M., King, J., Koc, N., Krylov, A., Martinez, N., Matthiessen, J., McInroy, D., Moore, T.W., Onodera, J., O'Regan, M., Pälike, H., Rea, B., Rio, D., Sakamoto, T., Smith, D.C., Stein, R., St John, K., Suto, I., Suzuki, N., Takahashi, K., Watanabe, M., Yamamoto, M., Farrell, J., Frank, M., Kubik, P., Jokat, W., Kristoffersen Y., 2006. The Cenozoic palaeoenvironment of the Arctic Ocean. Nature 441, 601–605.

Nix, H., 1982. Environmental determinants of biogeography and evolution in Terra Australis, in: Barker, W.R., Greenslade, P.J.M. (Eds.), Evolution of the flora and fauna of Arid Australia. Frewville, Peacock Publishing, pp. 47–66.

O'Regan, M., Moran, K., Backman, J., Jakobsson, M., Sangiorgi, F., Brinkhuis, H., Pockalny, R., Skelton, A., Stickley, C., Koç, N., Brumsack, H.-J., Willard, D., 2008. Mid-Cenozoic

tectonic and paleoenvironmental setting of the central Arctic Ocean. Paleoceanography 23, PA1S20, doi:10.1029/2007PA001559.

Phuphumirat, W., Zetter, R., Hofmann, C.-C., Ferguson, D.K., 2016. Pollen distribution and deposition in mangrove sediments of the Ranong Biosphere Reserve, Thailand. Rev. Palaeobot. Palynol. 233, 22–43.

Poirier, A., Hillaire-Marcel, C., 2011. Improved Os–isotope stratigraphy of the Arctic Ocean. Geophys. Res. Lett. 38, L14607, doi:10.1029/2011GL047953.

Ryan, W.B.F., Carbotte, S.M., Coplan, J.O., O'Hara, S., Melkonian, A., Arko, R., Weissel, R.A., Ferrini, V., Goodwillie, A., Nitsche, F., Bonczkowski, J., Zemsky, R., 2009. Global Multi-Resolution Topography synthesis, Geochem. Geophys. Geosyst. 10**,** Q03014, http://dx.doi.org/10.1029/2008GC002332.

Salpin, M., Schnyder, J., Baudin, F., Suan, G., Suc, J.-P., Popescu, S.-M., Fauquette, S., Reinhardt, L., Schmitz, M.D., Labrousse, L., 2019. Evidence for subtropical warmth in the Canadian Arctic (Beaufort-Mackenzie, Northwest Territories, Canada) during the early Eocene. Geol. Soc. Amer. Spec. Paper 541-27**,** 637–664.

Schouten, S., Eldrett, J., Greenwood, D.R., Harding, I., Baas, M., Damsté, J.S., 2008. Onset of long-term cooling of Greenland near the Eocene-Oligocene boundary as revealed by branched tetraether lipids. Geology 36, 147–150.

Sluijs, A., Röhl, U., Schouten, S., Brumsack, H.-J., Sangiorgi, F., Sinninghe Damsté, J.S., Brinkhuis, H., 2008. Arctic late Paleocene–early Eocene paleoenvironments with special emphasis on the Paleocene–Eocene thermal maximum (Lomonosov Ridge, Integrated Ocean Drilling Program Expedition 302). Paleoceanography 23, PA1S11, doi:10.1029/2007PA001495.

Sluijs, A., Schouten, S., Pagani, M., Woltering, M., Brinkhuis, H., Sinninghe Damsté, J.S., Dickens, G.R., Hubern M., Reichart, G.-J., Stein, R., Matthiessen, J., Lourens, L.J.,

Pedentchouk, N., Backman, J., Moran, K., and the Expedition 302 Scientists, 2006. Subtropical Arctic Ocean temperatures during the Paleocene/Eocene thermal maximum. Nature 441, 610–613.

Sluijs, A., Schouten, S., Donders, T.H., Schoon, P.L., Röhl, U., Reichart, G.-J., Sangiorgi, F., Kim, J.-H., Sinninghe Damsté, J.S., Brinkhuis, H., 2009. Warm and wet conditions in the Arctic region during Eocene Thermal Maximum 2. Nature Geoscience 2**,** 777–780.

Somboom, J.R.P., 1990. Palynological study of mangrove and marine sediments of the Gulf of Thailand. Journ. Southeast Asian Earth Sci. 4, 85–97.

St John, K., 2008. Cenozoic ice-rafting history of the central Arctic Ocean: Terrigenous sands on the Lomonosov Ridge. Paleoceanography 23, PA1S05, doi:10.1029/2007PA001483.

Staplin, F.L., 1976. Tertiary biostratigraphy, Mackenzie Delta region, Canada. Bull. Canadian Pet. Geol. 24, 117–136.

Stein, R., Jokat, W., Niessen, F., Weigelt, E., 2015. Exploring the long-term Cenozoic Arctic Ocean climate history: a challenge within the International Ocean Discovery Program (IODP). Arktos 1, 3 doi:10.1007/s41063-015-0012-x.

Stickley, C.E., St John, K., Koç, N., Jordan, R.W., Passchier, S., Pearce, R.B., Kearns, L.E., 2009. Evidence for middle Eocene Arctic sea ice from diatoms and ice-rafted debris. Nature 460, 376–379.

Suan, G., Popescu, S.-M., Suc, J.-P., Schnyder, J., Fauquette, S., Baudin, F., Yoon, D., Piepjohn, K., Sobolev, N.N., Labrousse, L., 2017. Subtropical climate conditions and mangrove growth in Arctic Siberia during the early Eocene. Geology 45, 539–542.

Suc, J.-P., Popescu, S.-M., Fauquette, S., Bessedik, M., Jiménez-Moreno, G., Bachiri Taoufiq, N., Zheng, Z., Médail, F., 2018. Reconstruction of Mediterranean flora, vegetation and climate for the last 23 million years based on an extensive pollen dataset. Ecologia mediterranea, 44, 2, 53–85.

Thompson, R.S., Anderson, K.H., Bartlein, P.J., 2000. Atlas of relations between climatic parameters and distributions of important trees and shrubs in North America. U.S. Geological Survey Professional Paper, 1650; vol. A, 269 pp; vol. B, 423 pp.; vol. C, 386 pp.

Tomlinson, P.B., 1986. The Botany of Mangroves, Cambridge Univ. Press, Cambridge.

Tripati, A., Darby, D., 2018. Evidence for ephemeral middle Eocene to early Oligocene Greenland glacial ice and pan-Arctic sea ice. Nature Comm. 9, 1038, 1–11.

Vandenberghe, N., Hilgen, F.J., Speijer, R.P., 2012. The Paleogene Period, in: Gradstein, F.M., Ogg, J.G., Schmitz, M.D., Ogg, G.M. (Eds.), The Geological Time Scale 2012. Elsevier, Amsterdam, pp. 855–921.

von Gosen, W., Reinhardt, L., Piepjohn, K., Schmitz, M.D., 2019. Paleogene sedimentation and Eurekan deformation in the Stenkul Fiord area of southeastern Ellesmere Island (Canadian Arctic): Evidence for a polyphase history. Geol. Soc. Amer. Special Paper 541-16**,** 325–348.

Weijers, J.W.H., Schouten, S., Sluijs, A., Brinkhuis, H., Sinninghe Damsté, J.S., 2007. Warm arctic continents during the Palaeocene–Eocene thermal maximum. Earth Planet. Sci. Lett. 261, 230–238.

Weller, P., Stein, R., 2008. Paleogene biomarker records from the central Arctic Ocean (Integrated Ocean Drilling Program Expedition 302): Organic carbon sources, anoxia, and sea surface temperature. Paleoceanography 23, PA1S17, doi:10.1029/200701001472.

West, C.K., Greenwood, D.R., Basinger, J.F., 2015. Was the Arctic Eocene 'rainforest' monsoonal? Estimates of seasonal precipitation from early Eocene megafloras from Ellesmere Island, Nunavut. Earth Planet. Sci. Lett. 427, 18–30.

Willard, D.A., Donders, T.H., Reichgelt, T., Greenwood, D.R., Sangiorgi, F., Peterse, F., Nierop, K.G.J., Frieling, J., Schouten, S., Sluijs, A., 2019. Arctic vegetation, temperature,

and hydrology during Early Eocene transient global warming events. Global Planet. Change 178, 139–152.

Willard, D.A., Weimer, L.M., Riegel, W.L., 2001. Pollen assemblages as paleoenvironmental proxies in the Florida Everglades. Rev. Palaeobot. Palynol. 113, 213–235.

**Figure captions**

Fig. 1. Location of the studied boreholes of Leg 302 (ACEX) and comparative pollen localities of Caribou Hills and Faddeevsky Island. The map is elaborated using GeoMapApp (Ryan et al., 2009).

Fig. 2. Detailed pollen diagram of boreholes M0004A and M0002A showing the ecological subdivision of taxa.

Percentages were calculated with respect to the number of identified pollen grains. The pollen diagram is interrupted for intervals without samples large of about 10 m or more because of unrecovered intervals (see: Backman et al., 2006) or unavailable sediment.

Fig. 3. Synthetic pollen diagram of boreholes M0004A and M0002A and proposed climatostratigraphic correlations of the warmest phases with the generalized oxygen isotope curve (Vandenberghe et al., 2012).

Classification of taxa constituting the pollen flora with reference to the thermal grouping of plants suggested by Nix (1982): megatherms, i.e. tropical plants, requiring a mean annual temperature greater than 24 °C; mega-mesotherms, i.e. subtropical plants, requiring a mean

annual temperature comprised between 20 °C and 24 °C; mesotherms, i.e. warm-temperate plants, growing under a mean annual temperature comprised between 14 °C and 20 °C; meso-microtherms, i.e. cool-temperate plants, growing under a mean annual temperature comprised between 12 °C and 14 °C; microtherms, i.e. boreal plants, growing under a mean annual temperature lower than 12 °C. Percentages of groups of plants are calculated with respect to the number of identified pollen grains minus those of *Pinus* and indeterminable Pinaceae. The pollen diagram and palaeoclimatic curves are interrupted for intervals without samples large of about 10 m or more because of unrecovered intervals (see: Backman et al., 2006) or unavailable sediment. Warmer and cooler phases are underlined by light and dark grey bands, respectively. Blue patches show the chief correlations between the pollen record and the oxygen isotope curve, blue dotted lines the subsidiary ones. Climatic values reconstructed from pollen data: mean annual temperature, mean temperature of the coldest month, mean temperature of the warmest month, annual precipitation. The records of *Azolla* isolated microspores and microspore massulae are indicated in green: the youngest record corresponds to the *Azolla* phase (Brinkhuis et al., 2006).

PETM, Paleocene–Eocene Thermal Maximum; ETM, Eocene Thermal Maximum; EECO, Early Eocene Climatic Optimum; MECO, Mid Eocene Climatic Optimum.

Fig. 4. Curves of sedimentation rate estimated from our results for the studied parts of boreholes M0004A (in red) and M0002A (in blue) compared to previous calculations in grey (Backman et al., 2006) and black (Poirier and Hillaire-Marcel, 2011) for its deviating course from the previous one. The age of the *Azolla* phase is re-evaluated.

PETM, Paleocene–Eocene Thermal Maximum; ETM, Eocene Thermal Maximum; EECO, Early Eocene Climatic Optimum; MECO, Mid Eocene Climatic Optimum.

Fig. 5. Palaeogeographic sketch slightly modified from a previous map (Eberle and Greenwood, 2008) illustrating the pollen transport to ACEX sedimentary sites from coastal part of lands for thermophilous plants. The blue arrow indicates the fluvial transport for pollen grains of altitudinal trees from the Ellesmere Range.

Table 1. Depths and ages considered for estimating the sedimentation rate of the studied parts of boreholes M0004A and M0002A.

| Hole | Reference dot | Depth (mcd) | Age (Ma) |
|---|---|---|---|
| M0002A | Top of the study | 221.025 | 40 |
| | MECO | 232.39 | 40.3 |
| | Base of the study | 263.815 | 42 |
| M0004A | Top of the study | 270.12 | 48 |
| | Top EECO | 282.055 | 48.8 |
| | Base upper EECO | 292.285 | 49.5 |
| | Top lower EECO | 313.41 | 50 |
| | Base EECO | 318.86 | 51.4 |
| | ETM2 | 368.24 | 53.8 |
| | PETM | 382.44 | 55.84 |
| | Base of the study | 401.31 | 57 |

- Spread of subtropical *Avicennia* mangrove and evergreen forest indicates warmer phases
- Climatostratigraphy allows identification of PETM, EECO and MCO as major warm phases
- The *Azolla* phase was a local event during a climatically unstable episode within EECO
- Lands existed along the Lomonosov Ridge in connection with the Ellesmere Range

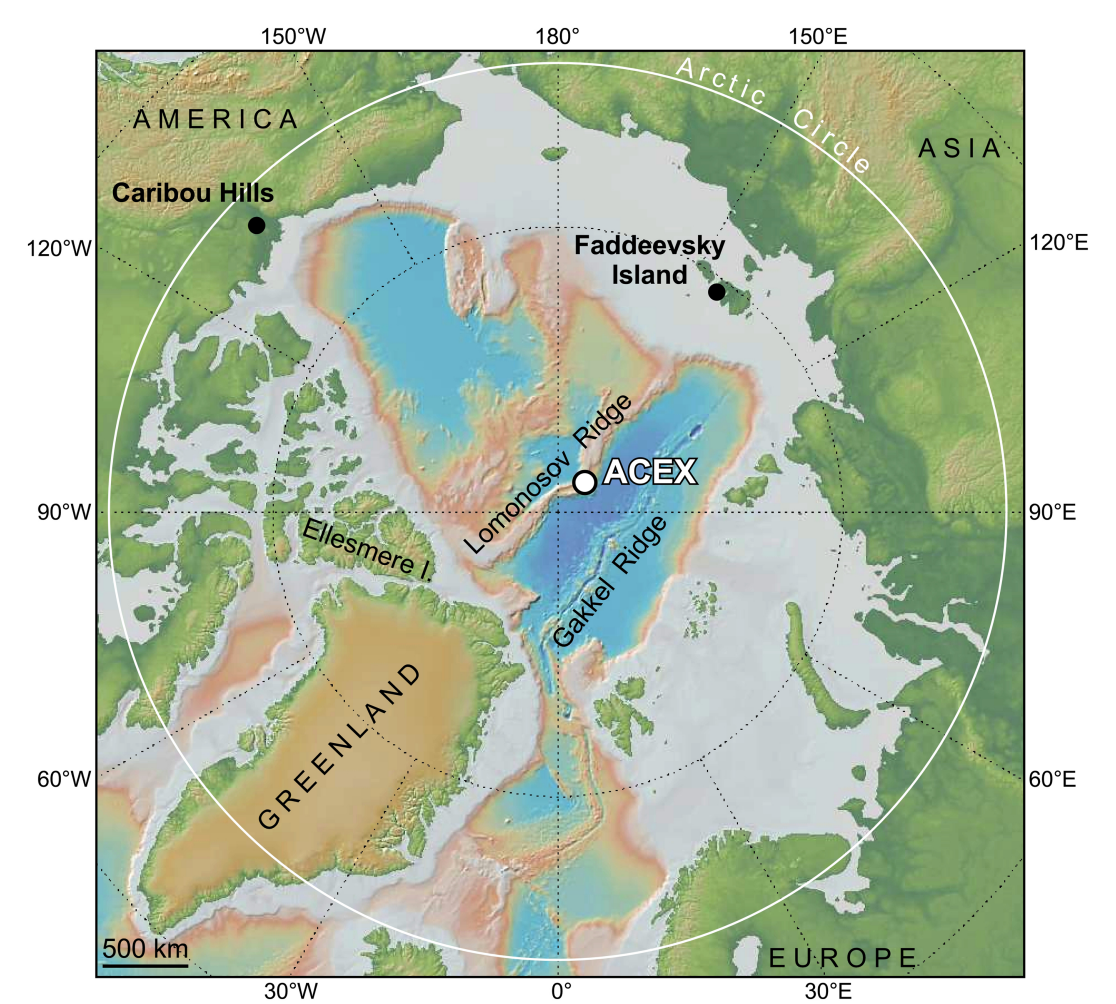
150°W
180°
150°E
AMERICA
Arctic Circle
ASIA
Caribou Hills
Faddeevsky Island
120°W
120°E
Lomonosov Ridge
ACEX
90°W
90°E
Ellesmere I.
Gakkel Ridge
GREENLAND
60°W
60°E
500 km
EUROPE
30°W
0°
30°E

Figure 1

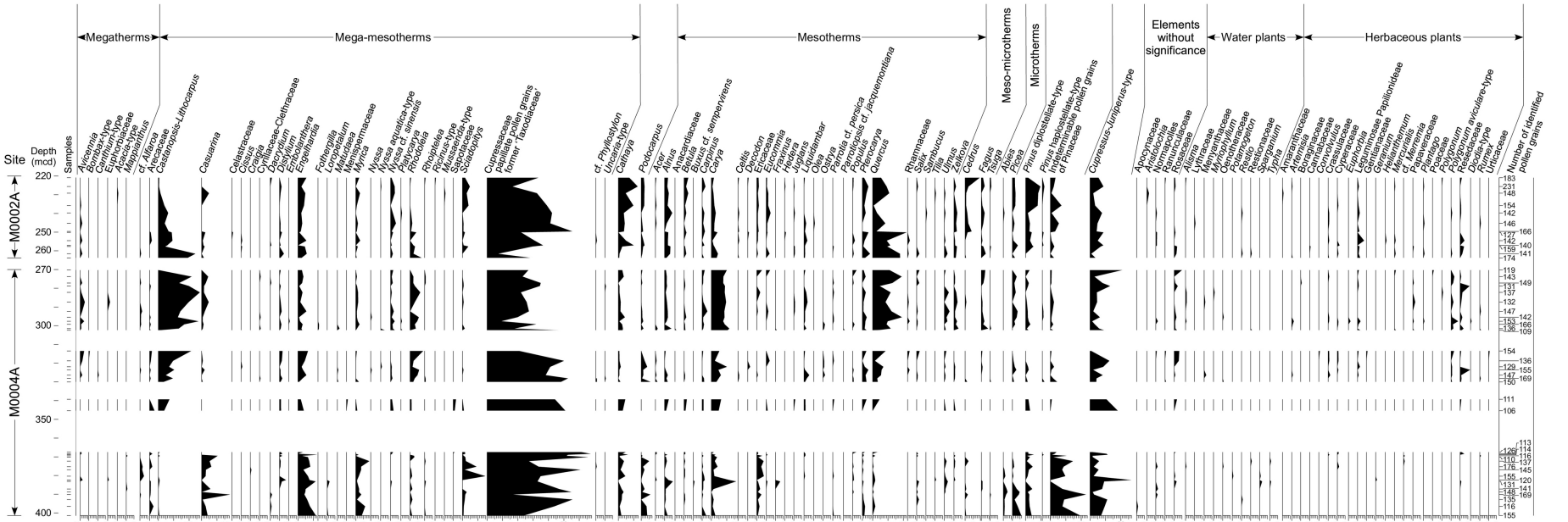
Megatherms
Mega-mesotherms
Mesotherms
Meso-microtherms
Microtherms
Elements without significance
Water plants
Herbaceous plants
Site
Depth (mcd)
Samples
M0002A
M0004A
Number of identified pollen grains

Figure 2

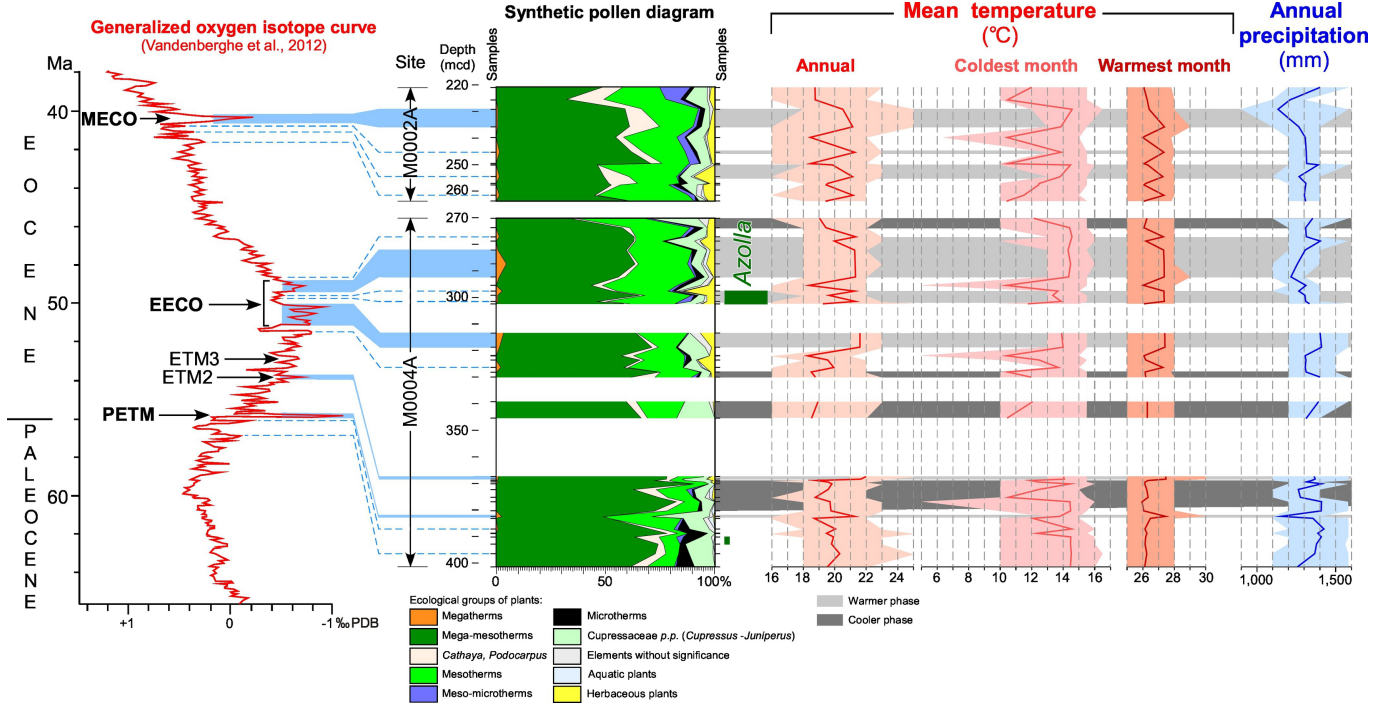
Generalized oxygen isotope curve
(Vandenberghe et al., 2012)
Ma
40
50
60
EOCENE
PALEOCENE
MECO
EECO
ETM3
ETM2
PETM
+1
0
-1 ‰PDB
Site
Depth (mcd)
Samples
Samples
M0002A
M0004A
220
250
260
270
300
350
400
Azolla
0
50
100%
Synthetic pollen diagram
Mean temperature (°C)
Annual
Coldest month
Warmest month
Annual precipitation (mm)
16 18 20 22 24
6 8 10 12 14 16
26 28 30
1,000
1,500
Ecological groups of plants:
Megatherms
Mega-mesotherms
Cathaya, Podocarpus
Mesotherms
Meso-microtherms
Microtherms
Cupressaceae p.p. (Cupressus -Juniperus)
Elements without significance
Aquatic plants
Herbaceous plants
Warmer phase
Cooler phase

Figure 3

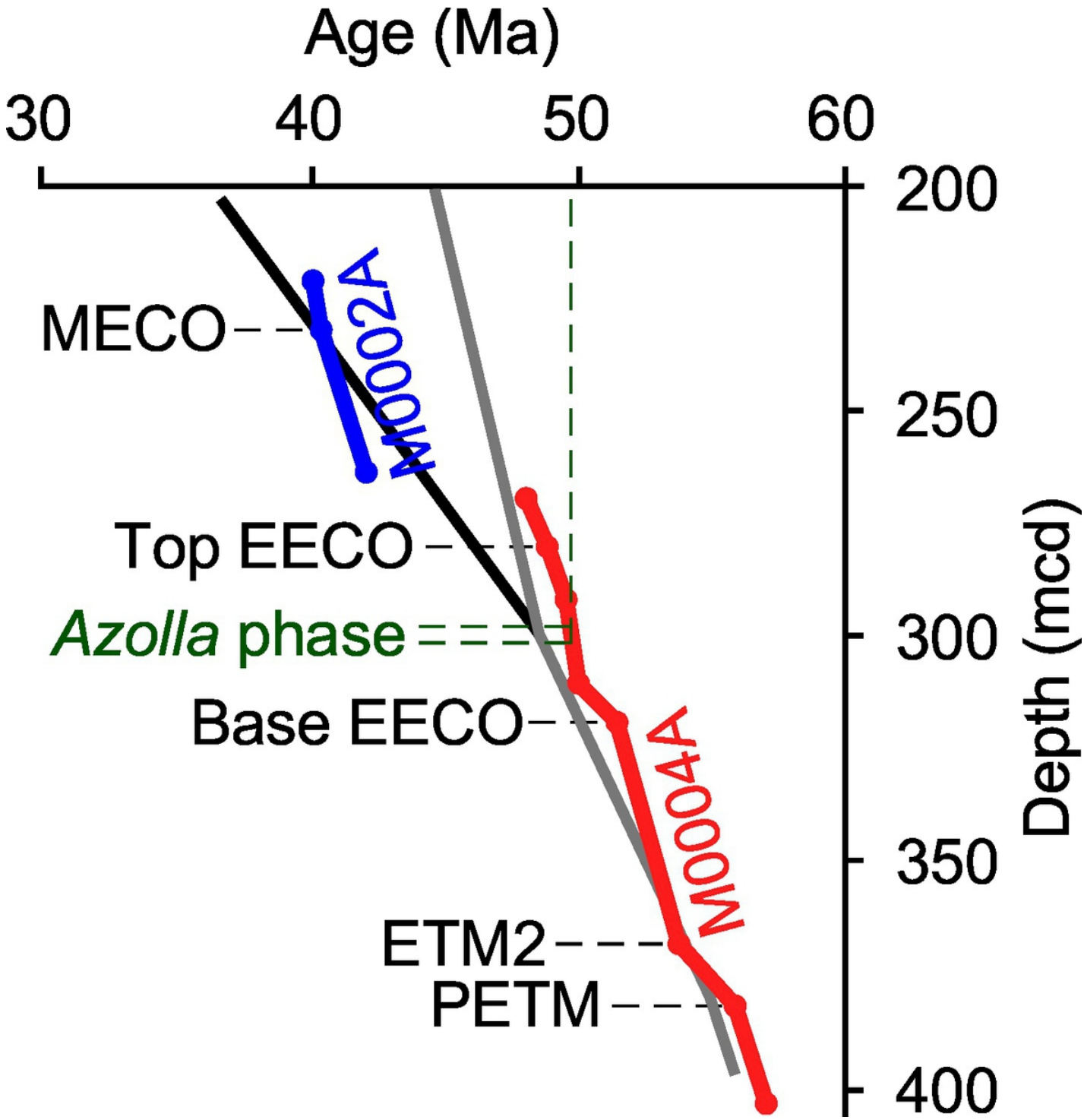
Age (Ma)
30
40
50
60
200
250
300
350
400
Depth (mcd)
MECO
Top EECO
Azolla phase
Base EECO
ETM2
PETM
M0002A
M0004A

Figure 4

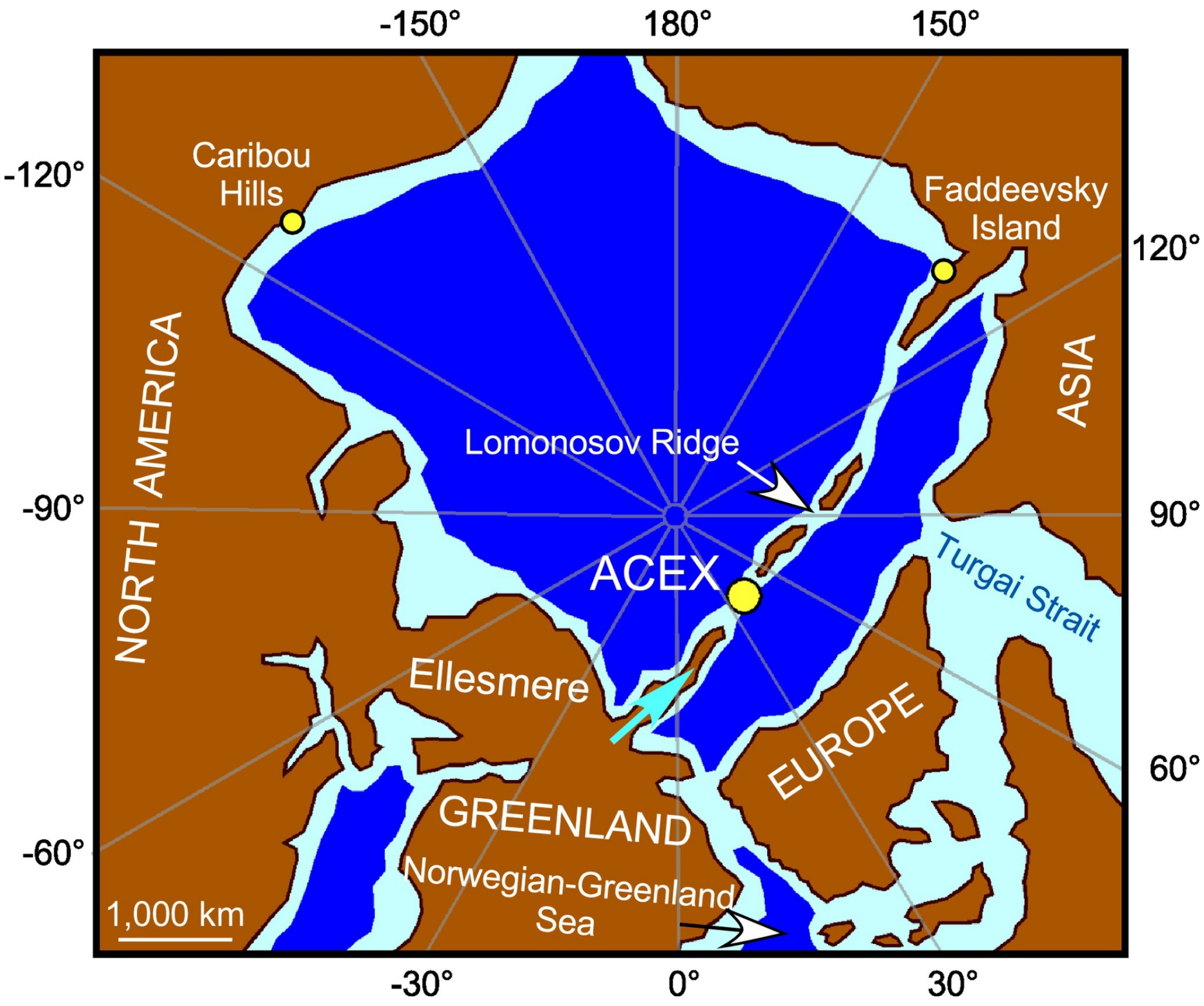
-150°
180°
150°
-120°
120°
-90°
90°
-60°
60°
-30°
0°
30°
Caribou Hills
Faddeevsky Island
NORTH AMERICA
ASIA
Lomonosov Ridge
ACEX
Turgai Strait
Ellesmere
EUROPE
GREENLAND
Norwegian-Greenland Sea
1,000 km

Figure 5